

# Growth and band gap determination of the $\text{ZrS}_x\text{Se}_{2-x}$ single crystal series

Mohamed Moustafa, Thorsten Zandt, Christoph Janowitz, and Recardo Manzke  
 Institut für Physik, Humboldt-Universität zu Berlin, Newtonstr. 15, D-12489 Berlin, Germany  
 (Received 4 May 2009; published 28 July 2009)

Single crystals of layered transition-metal dichalcogenide compounds of  $\text{ZrS}_x\text{Se}_{2-x}$  with composition  $0 \leq x \leq 2$  were grown by the chemical-vapor-transport technique and characterized with the help of different methods. Indirect gap transitions with remarkably high values of the absorption coefficient  $\alpha(h\nu)$  and the energy-gap values have been extracted from the optical-absorption measurements. An approximate linear dependence of the band gaps on the composition parameter  $x$  has been observed, qualifying them to become promising candidates for band gap engineering. The range of the obtained band gaps, which varies from 1.18 eV for  $\text{ZrSe}_2$  to 1.7 eV for  $\text{ZrS}_2$ , is suitable for photovoltaic applications in both single- and multiple-junction cells. Additionally, a significant absorption-coefficient tail near the fundamental absorption edge is discussed, which is found to obey the Urbach rule.

DOI: 10.1103/PhysRevB.80.035206

PACS number(s): 78.40.Fy, 71.35.Cc, 81.10.Bk

## I. INTRODUCTION

Among many semiconducting materials investigated for photovoltaic solar-cell applications, e.g., Si, CdS, CdTe, CuInSe<sub>2</sub>,<sup>1,2</sup> and GaInP/GaAs/Ge for tandem cells,<sup>3</sup> transition-metal dichalcogenide (TMDC) materials have attracted a remarkable degree of attention due to their comprehensive attractive properties. They are cheap and abundant, available in both  $n$ - and  $p$ -type forms, have energy-band gaps well suited to solar-energy conversion, a high absorption coefficient in the visible range, the tendency to grow as thin films, and they are nontoxic materials. These superior properties qualify them as potential candidates for photovoltaic applications. For example, molybdenum and tungsten sulphoselenide compounds have been proven to be very attractive semiconducting materials for the use in photoelectrochemical energy-conversion processes.<sup>4,5</sup> Zirconium dichalcogenides showed the possibility to be used in solid-state solar-cell technology and devices; they also exhibit some interesting switching and memory effects.<sup>6</sup>

The compounds of these materials have the common formula  $\text{MX}_2$  where  $M$  is a transition metal of groups IVb, Vb, and VIb and  $X$  is one of the chalcogens S, Se, or Te. The most striking feature of these compounds is that they crystallize in a quasi-two-dimensional structure consisting of a sheet of metal atoms sandwiched between two sheets of chalcogens forming  $X\text{-M-X}$  layers with strong mixed covalent-ionic intralayer bonding while the interlayer bonding is of the relatively weak Van der Waals type. This two-dimensional bonding behavior is responsible for the marked anisotropy in a number of their physical properties. Several studies on the structure,<sup>7</sup> optical,<sup>8,9</sup> and electronic properties<sup>10,11</sup> have been performed for these layer-type structure compounds.

The TMDC materials we are concerned with here are from the  $\text{ZrS}_x\text{Se}_{2-x}$  series. They are materials of the group IVb with transition metal Zr and chalcogens S and Se, and crystallize in a layered  $1T$  structure in which the transition metal is octahedrally coordinated by six chalcogenide atoms [Fig. 1(a)]. The electron configuration of the transition metal Zr in the  $\text{ZrS}_x\text{Se}_{2-x}$  is  $4d^25s^2$  and that of both chalcogens S

and Se is  $s^2p^4$ , i.e., both missing two electrons for a filled shell. Therefore, the two chalcogen atoms per f.u. may attract a total of four transition-metal  $d$  electrons ( $d_0$  configuration)

$$M_{d^2s^2} + 2C_{s^2p^4} \rightarrow M_{d^0s^0} + 2C_{s^2p^6} \quad (1)$$

The  $p$  orbitals of the chalcogenides and the  $s/p$  orbitals of the metal form bonding  $\sigma$  and antibonding  $\sigma^*$  bands, resulting in a gap between 5 and 10 eV. The  $d$  states of the transition metal are located within this gap. They are split due to the ligand field and a trigonal distortion. The  $d_{xz}$  and  $d_{yz}$  orbitals are repelled by the  $p_x$  and  $p_y$  orbitals of the chalcogen

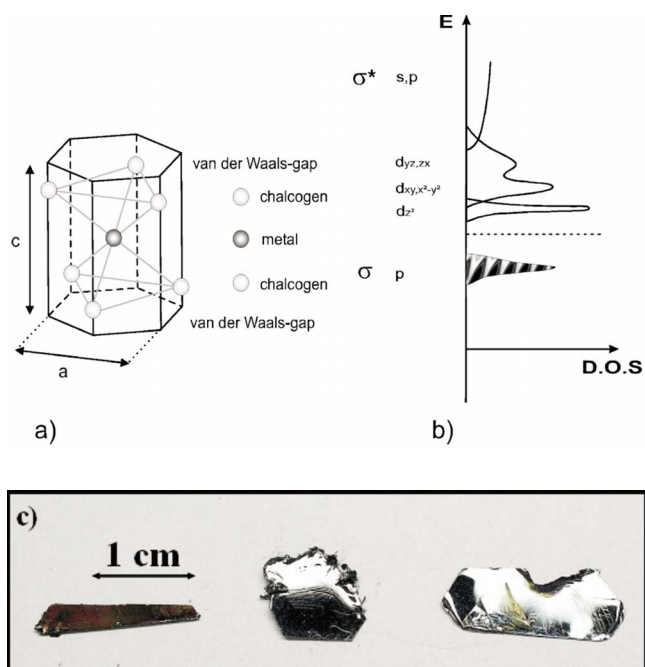


FIG. 1. (Color online) (a)  $1T$  structure with the octahedrally coordinated transition metal of TMDC materials. (b) Band model for the group-IVB TMDC of Friend and Yoffe (Ref. 12). DOS is the density of state, for other characters see the text. (c) Examples of the obtained single crystals grown by CVT technique. From left:  $\text{ZrSe}_2$ ,  $\text{ZrSSe}$ , and  $\text{ZrS}_{1.8}\text{Se}_{0.2}$ .

TABLE I. Growth conditions of single crystals of the series  $ZrS_xSe_{2-x}$ .

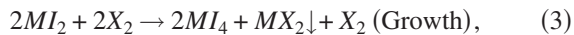
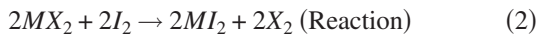
Compound	$\pm x$	Reaction temperature (°C)	Growth temperature (°C)	Reaction time (h)	Color
ZrSe <sub>2</sub>	0	900	810	350	Bronze green
ZrS <sub>0.3</sub> Se <sub>1.7</sub>	0.06	900	815	200	Metallic green
ZrS <sub>0.8</sub> Se <sub>1.2</sub>	0.04	900	810	210	Metallic green
ZrSSe	0.04	900	820	200	Not specified
ZrS <sub>1.5</sub> Se <sub>0.5</sub>	0.06	910	825	200	Not specified
ZrS <sub>1.7</sub> Se <sub>0.3</sub>	0.05	900	825	200	Metallic
ZrS <sub>1.8</sub> Se <sub>0.2</sub>	0.05	895	818	300	Metallic
ZrS <sub>2</sub>	0.04	950	800	250	Metallic red

genides, therefore they are energetically on the highest level, and both  $d_{x^2-y^2}$  and  $d_{xy}$  orbitals are repelled by the  $p_z$  chalcogenide orbital. The most interesting orbital at lowest energy is that with  $d_z^2$  symmetry. In group IVb TMDC  $ZrS_xSe_{2-x}$  it is unoccupied and forms the lowest conduction band whereas in the groups Vb and VIb TMDC materials are half and totally filled, respectively. Therefore, it is of importance in determining the character of the TMDC materials. Figure 1(b) shows the resulting band model as proposed by Friend and Yoffe.<sup>12</sup>

The electronic band structure and the band gap values have been studied theoretically and experimentally only for the end members of the  $ZrS_xSe_{2-x}$  series, i.e., ZrSe<sub>2</sub> and ZrS<sub>2</sub>. All calculations carried out by different methods<sup>13-16</sup> revealed that both materials are indirect semiconductors with relatively large energy gaps due to the quite weak  $p-d$  interactions. The valence-band maximum (VBM) is located at the  $\Gamma$  point and the conduction-band minimum (CBM) lies midway between  $\Gamma$  and  $K$  points of the Brillouin zone. The band gaps determined experimentally exist as well only for the end members ZrSe<sub>2</sub> of 1.2 eV (Ref. 9) and ZrS<sub>2</sub> of 1.68 (Ref. 8) and 1.7 eV.<sup>9</sup> In this work, we report the growth of single crystals and the energy-gap variation in different compositions of the ternary compounds series of  $ZrS_xSe_{2-x}$ . Additionally, an interpretation of the absorption tail observed near the absorption edge is reported.

## II. EXPERIMENTS

All  $ZrS_xSe_{2-x}$  crystals were grown by utilizing the chemical-vapor-transport technique (CVT) using iodine as the transport agent, similar to the method used by Rimington and Balchin in the growth of tin sulphoselenides and zirconium sulphoselenides.<sup>17</sup> Over a period of several days two reactions take place according to



$M$  represents here the group IV transition-metal zirconium and  $X$  represents the chalcogens. The stoichiometric quantities of sulfur powder (99.999% purity), selenium powder (99.999% purity), and zirconium (purity of 99.8%) were

placed in quartz ampoules which were 200-mm long and 15 mm in diameter. Iodine (purity of 99.999%) was added to provide an iodine concentration of 5 mg cm<sup>-3</sup> of the ampoule volume. The charged ampoules were evacuated and sealed at a pressure of approximately  $2 \times 10^{-5}$  Torr with the reagents maintained at liquid-nitrogen temperature. Crystal growth took place in a four-zone horizontal furnace, two of them used as buffer zones to avoid thermal disturbance from the outside. The charged ampoules were placed in the central region of the furnace with the charged end located at the higher temperature (reaction zone) and the empty end located at the lower temperature (growth zone). The furnace temperatures were slowly increased with an approximate rate of 50 °C/h and the temperature gradient between the growing zones was almost linear. The details of growth conditions and the results are given in Table I. The growth conditions were found to be critical, thus small variation in the temperature values caused an additional existence of ZrS<sub>3</sub> needles.

Using the CVT technique, single crystals of size up to  $20 \times 10$  mm<sup>2</sup> in the superficial area showing good cleavage properties in the direction perpendicular to the  $c$  axis were obtained Fig. 1(c). Although the colors of the various crystals are thickness dependent, in general they change their color from red (disulphides) to bronze green (diselenides). The compositions of the as-grown crystals were determined using energy dispersive x-ray emission (EDX). The deviations from the nominal compositions  $\pm x$  are given in Table I. The thickness of the crystals was measured by an electron microscope (Cambridge Instruments S360). An example of uncleaved  $ZrS_{1.7}Se_{0.3}$  crystals is shown in Fig. 2(a). For a qualitative determination of the structure low-energy electron diffraction (LEED) (VG Microtech RVL 900) [Fig. 3(b)] and Laue diffraction patterns were taken. For the purpose of optical properties analysis, the measurements of the transmission were performed by a prism monochromator (Carl Zeiss Jena) and a computer using a high-precision digital voltmeter (Schlumberger technologies 7071). For all crystals the measurements were taken at room temperature. The reflectance  $R/R_o$  was found to be nearly constant over the whole wavelength region used and the transmittance  $T/T_o$  was normalized by incident light beam.

## III. RESULTS AND DISCUSSION

The absorption coefficient  $\alpha(\lambda)$  was determined from the measured transmittance  $T(\lambda)$ , after properly correcting for

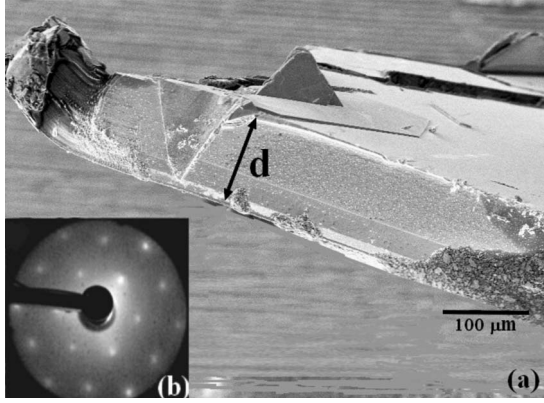


FIG. 2. (a) Image of  $\text{ZrS}_{1.7}\text{Se}_{0.3}$  taken by a scanning electron microscope. (b) LEED pattern of  $\text{ZrSe}_2$  at electron energy of 119 eV.

the reflectance  $R(\lambda)$ . The equation describing the wavelength transmittance dependence is given by

$$T(\lambda) = \frac{T}{T_o} \cong \frac{[1 - R(\lambda)]^2 e^{-\alpha(\lambda)d}}{1 - R(\lambda)^2 e^{-2\alpha(\lambda)d}}, \quad (4)$$

where  $d$  is the specimen thickness. However, since the value of  $(\alpha d)$  is sufficiently high, Eq. (4) can be approximated to<sup>8</sup>

$$\alpha(\lambda) \cong \frac{1}{d} \{-\ln T(\lambda) + 2 \ln[1 - R(\lambda)]\}. \quad (5)$$

The absorption coefficient spectra extracted from the above equation are plotted in Fig. 3 for different values of  $x$  of our series. The graph exhibits a notable shift toward higher energy with increase in the relative amount of sulfur and the values of the absorption coefficient in this photon-energy region are in the range of  $10^3 \text{ cm}^{-1}$ . For example obtained values for  $\text{ZrSe}_2$ ,  $\text{ZrSSe}$ , and  $\text{ZrS}_2$  with thickness  $11.8 \pm 1\%$ ,  $11.3 \pm 1\%$ , and  $7.3 \pm 1\%$  in  $\mu\text{m}$  are  $6.97 \times 10^3$ ,  $6.77 \times 10^3$ , and  $8.18 \times 10^3$  in  $\text{cm}^{-1}$ , respectively. These values appear to be larger than those of the well-known indirect transitions

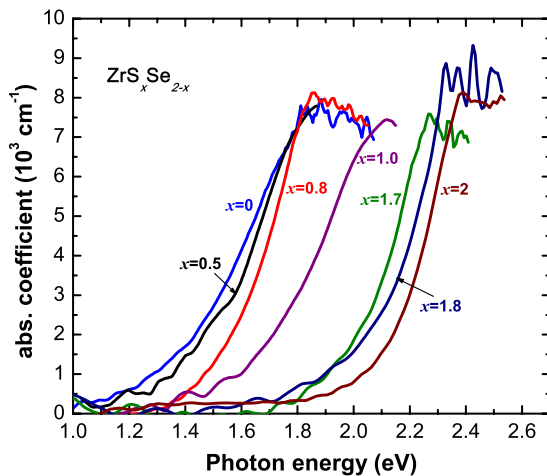


FIG. 3. (Color online) Plot of the absorption coefficient in the range of the energy gap for different composition  $x$  for the series  $\text{ZrS}_x\text{Se}_{2-x}$ .

but still much smaller than the typical value of the direct allowed transition of order  $10^5 \text{ cm}^{-1}$ .

The band gap values of the crystals were determined by analyzing the energy dependence of the absorption coefficient  $\alpha(h\nu)$  according to<sup>18</sup>

$$\alpha(h\nu) = \text{Const} \times f_B \int_0^{-h\nu - E_g \pm E_p} N(E_i)N(E_f)dE_i \quad (6)$$

$N(E_i)$  and  $N(E_f)$  are the density of the initial and final states, respectively, and  $f_B$  is the Einstein-Bose function that accounts for the distribution of the involved phonons with energy  $E_p$ . For isotropic structures the density of states behaves like

$$N(E_i) \sim \sqrt{|E_i|}, \quad N(E_f) \sim \sqrt{h\nu - E_g \pm E_p + E_i}. \quad (7)$$

Solving Eq. (6) by employing Eq. (7), the absorption coefficient at constant temperature ( $\alpha h\nu$ ) will be given by<sup>10</sup>

$$(\alpha h\nu) \sim (h\nu - E_g)^r. \quad (8)$$

For direct transitions, where  $r=1/2$  for allowed transitions and  $r=3/2$  for forbidden transitions, and

$$(\alpha h\nu) \sim (h\nu - E'_g \pm E_p)^r. \quad (9)$$

For indirect transitions, where  $r=2$  for allowed transitions and  $r=3$  for forbidden transitions.

$E_g$  and  $E'_g$  correspond to the direct and indirect energy gaps, respectively.  $E_p$  is the energy of the absorbed (+) or emitted (-) phonon. Based on our observation of a rather low-absorption coefficient for the mixed crystals of the  $\text{ZrS}_x\text{Se}_{2-x}$  series as well as on previously reported experimental and theoretical data of the end members of the series  $\text{ZrSe}_2$  and  $\text{ZrS}_2$  we made our further analysis under the assumption of indirect-gap semiconductors.

For the determination of the band gaps,  $(\alpha h\nu)^r$  is plotted against  $h\nu$  where the values of the energy gap were obtained by extrapolating the linear part of the plot of the absorption coefficient till the intersection with the photon energy axis. Figure 4(a) illustrates an example of the deduction in the indirect band gap values, whereas Fig. 4(b) is for the determination of direct band gaps. The results for different compositions are given in Table II together with other experimental and calculated values. The obtained energy-gap values of the end members  $\text{ZrS}_2$  and  $\text{ZrSe}_2$  are in a good agreement with the previously published experimental results. For example the value of 1.68 eV for  $\text{ZrS}_2$  deduced from reflection data by Greenaway and Nitsche,<sup>8</sup> and 1.7 and 1.2 eV for  $\text{ZrS}_2$  and  $\text{ZrSe}_2$  respectively obtained from transmission measurements by Lee *et al.*<sup>9</sup> But as no previous data are available for the rest of the series of  $\text{ZrS}_x\text{Se}_{2-x}$  a similar comparison could not be made. However, the agreement with the absolute values of the band gaps obtained from the calculations is less satisfactory, nevertheless the difference in the band gap values between the end members of  $\sim 0.52 \text{ eV}$  compares well with the reported value of  $\sim 0.55 \text{ eV}$  from theory.<sup>13</sup>

The determined energy-gap values for the different compositions of the  $\text{ZrS}_x\text{Se}_{2-x}$  family are plotted as a function of composition  $x$  in Fig. 5. It is seen that the energy-gap values

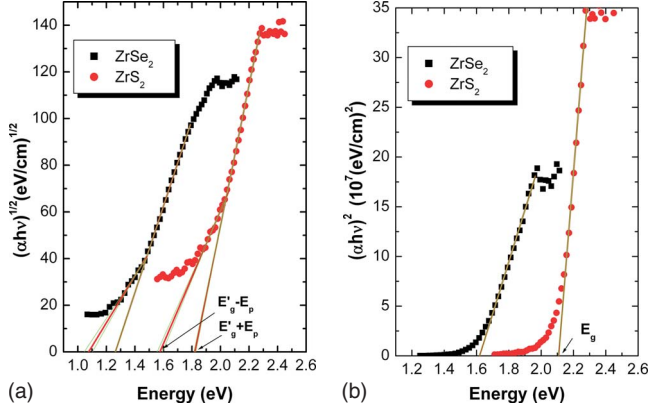


FIG. 4. (Color online) Dependence of  $(ah\nu)^r$  on the photon energy ( $h\nu$ ) for both  $\text{ZrSe}_2$  and  $\text{ZrS}_2$ . Extrapolating the linear part of each curve toward energy axis gives the corresponding energy band gap. (a)  $r=\frac{1}{2}$  for indirect transition and (b)  $r=2$  for direct transition. (Broken lines depict the error bound).

have an approximately linear proportionality to the composition parameter  $x$ , consistent with earlier observed behavior for other mixed compound semiconductors, e.g.,  $\text{SnS}_x\text{Se}_{2-x}$  (Ref. 9) and  $\text{HfS}_x\text{Se}_{2-x}$ .<sup>19</sup> This nearly linear dependence of energy gap with composition could be interpreted as follows. A linear variation indicates that the members of the component materials have a similarity in the band structures. Recently published band-structure calculations support this view. For example, Reshak and Auluck<sup>13</sup> showed that both  $\text{ZrS}_2$  and  $\text{ZrSe}_2$  have a very similar band structure with only minor differences. Therefore, this is also expected for the other members of the family. On the other hand, if the band structures are different, an abrupt change in slope in the energy gap vs composition relationship may be seen at some intermediate points, this was observed in other compounds, for example in Ge-Si alloys and  $\text{Bi}_2\text{Te}_3$ - $\text{Bi}_2\text{Se}_3$  alloys.<sup>20</sup>

Moreover, sulfur is a nonmetal and less conducting than the other two elements Se and Zr, that renders the compound to be more resistive with the increase in the sulfur content, i.e.,  $x$  in  $\text{ZrS}_x\text{Se}_{2-x}$ , hence increasing band gap with  $x$ .<sup>21</sup> Further, there is a difference in the electronegativity  $\varepsilon$  of the

TABLE II. Energy gap values for the  $\text{ZrS}_x\text{Se}_{2-x}$  series.  $E_g$  and  $E'_g$  are direct and indirect values, respectively. (Values without references=this work).

$\text{ZrS}_x\text{Se}_{2-x}$ $x$	Expt.		Theory $E'_g$
	$E_g$ (eV)	$E'_g$ (eV)	
0.0	1.61	1.2 (Ref. 9), 1.18	1.37 (Ref. 14), 1.0 (Ref. 15), 0.98 (Ref. 7), 0.85 (Ref. 13)
0.3	1.66	1.20	
0.8	1.72	1.26	
1.0	1.80	1.40	
1.7	1.95	1.58	
1.8	2.00	1.63	
2.0	2.10	1.68 (Ref. 8), 1.7	1.78 (Ref. 16), 1.6 (Ref. 7), 1.4 (Ref. 13)

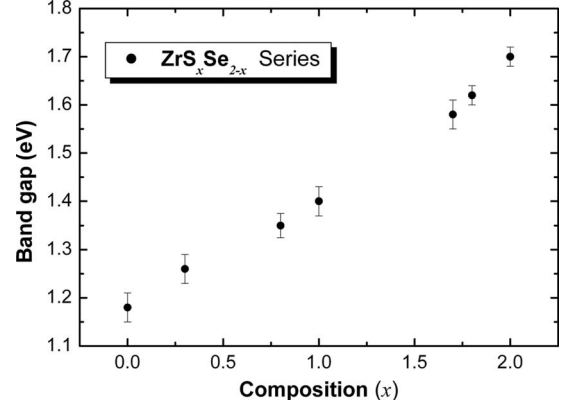


FIG. 5. Band gap values vs the composition  $x$  for the TMDC series  $\text{ZrS}_x\text{Se}_{2-x}$ .

chalcogenides i.e.,  $\varepsilon_S > \varepsilon_{\text{Se}}$  which makes  $\text{ZrS}_2$  more ionic than  $\text{ZrSe}_2$ , leading to a larger band gap values. In conclusion, we might ascribe the nearly linear dependence of the band gap on  $x$  to the linear change in the electronegativity of the chalcogenide<sup>19</sup> and to the similarity of the band structure of the Zr series having the VBM at the  $\Gamma$  point and the CBM at midway between  $\Gamma$  and  $K$  of the Brillion zone.

#### IV. URBACH TAIL

An exponentially increasing absorption edge rather than a steeply rising one, near the absorption edge, has been found in a wide variety of materials such as insulators including ionic crystals, semiconductors, and organic crystals. It obeys the following empirical expression:<sup>22</sup>

$$\alpha = \alpha_0 e^{(E-E_0/E_U)}, \quad (10)$$

where  $\alpha_0$  and  $E_0$  are characteristic parameters of the material,  $E=\hbar\omega$  and  $E_U$  are the photon energy and the Urbach energy, respectively. This empirical rule was introduced by Urbach<sup>22</sup> for silver halides with an indirect band gap and for alkali halides with direct band gap. That is why it is called ‘‘Urbach’s rule’’ and absorption tails obeying this rule are called the ‘‘Urbach tails.’’ This absorption tail implies that there is a residual absorption at photon energies below the absorption edge. Although a number of theoretical studies were launched to explain the origin of the Urbach tail, it is probably true to say that yet there is no one unique explanation for this behavior. For example, Sumi and Toyozawa<sup>23</sup> and Abay et.al.<sup>24</sup> attribute the absorption tail to the interaction of electrons/excitons with phonons in the semiconductors. Cody *et al.*<sup>25</sup> and Ho *et al.*<sup>26</sup> suggest that the residual absorption below the absorption edge most probably originates from the temperature-independent static disorder and indicates the existence of impurities, dislocations, stacking faults, etc., in the layered materials.

According to Eq. (10), we have fitted Urbach’s tail of the absorption edge for some compositions of our crystals at room temperature. A very good fit [solid lines in Fig. 6(a)] to the experimental results can be obtained. From the fits, we obtain the Urbach energy  $E_U$  for our crystals. In Eq. (10)  $E_U=k_B T/\sigma$ , where  $k_B$  is the Boltzman constant,  $T$  is the

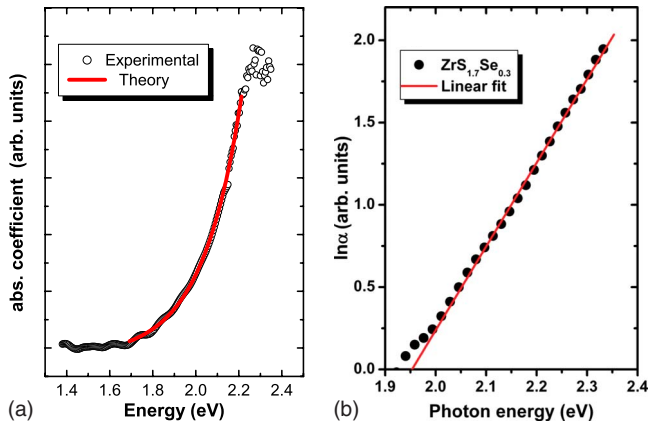


FIG. 6. (Color online) (a) Urbach's absorption tail. The solid lines represent the best fit to the obtained experimental data according to Eq. (10). (b)  $\ln \alpha$  versus the photon energy. For details see discussion in text. Both are for the  $\text{ZrS}_{1.7}\text{Se}_{0.3}$  crystals.

temperature, and  $\sigma$  is the so-called steepness parameter which characterizes the steepness or width of the straight line near the absorption edge. Equation (10) implies that the plots of the  $(\ln \alpha)$  vs photon energy near the absorption edge can be represented by an approximated straight line for energies just below the fundamental absorption edge, shown in Fig. 6(b).

The deduced values of the steepness parameter  $\sigma$  at room temperature for the investigated samples vary from  $(0.112 \pm 0.03)$  for  $\text{ZrSe}_2$  to  $(0.155 \pm 0.02)$  for  $\text{ZrS}_2$  corresponding to Urbach energy values of 235 and 190 meV, respectively. As the energy of phonons associated with the Urbach tail is an important parameter for the analysis, we have estimated the phonon energy from  $(\alpha h\nu)^{1/2}$  versus  $h\nu$  plots. Phonon energies values of 80 meV for  $\text{ZrSe}_2$  and 90 meV for  $\text{ZrS}_2$ , respectively, have been estimated. These values are in the same range of the earlier reported data of the same compounds [ $\sim 70$  meV for  $\text{ZrS}_2$  (Ref. 8)] and also of other layered indirect semiconductors [ $\sim 56$  meV for  $\text{Ti}_2\text{GaInSe}_4$  (Ref. 27)]. From the relatively large obtained Urbach energy values, it is strongly suggested that, both exciton/electron-phonon interactions, and the structural and compositional disorder contribute to cause the Urbach tail for our crystals. This relation between the width of the Urbach energy and the cause of this behavior has been experimentally and theoretically proven,<sup>25</sup> i.e., larger values of  $E_U$  is due to both interaction factors rather than one. Further, the estimated phonon energy values are relatively high which indicates that there is a contribution to the absorption edge from structural and compositional disorder. This view agrees well with the em-

pirical model proposed by Yang *et al.*<sup>28</sup> which takes into account, in addition to the influence of electron/exciton-phonon interactions, the electronic distortion which leads to higher values of the phonon energy due to structural and compositional disorder. The same behavior was also observed for another layered semiconductor with indirect band gap viz  $\text{MoSe}_2$  where the both factors contribute comparable to the observed Urbach width at room temperature.<sup>29</sup> The larger values of the observed Urbach energy for  $\text{ZrSe}_2$  compared to  $\text{ZrS}_2$  may be attributed to higher disorder and impurities in our Se compounds than in the S compounds. This behavior has already been reported for other layered semiconducting dichalcogenides composites of selenium and sulfur.<sup>23,26</sup> From the above discussion it can be concluded that the Urbach tail observed in our mixed crystals is due to both temperature-independent (static structural disorder) and electron/exciton-phonon-induced interactions (dynamic phonon disorder) contributions.

## V. CONCLUSIONS

The chemical-vapor-transport technique has been used to grow relatively large-size single crystals of the  $\text{ZrS}_x\text{Se}_{2-x}$  series. The crystals are two-dimensional semiconductors with indirect bandgap. Band gap values for the  $\text{ZrS}_x\text{Se}_{2-x}$  series have been determined from the energy dependence of the absorption coefficient. The obtained band gap values show a nearly linear proportionality to the composition parameter  $x$ , which can be understood in terms of similar electronic structure and the changing electronegativity of the members of the series. In favor of applications, the similarity of the band structure and the linear dependence of the gap values with  $x$  qualify them as competitive materials for photovoltaics and band gap engineering. Furthermore, the absorption coefficient near the fundamental absorption edge is energy dependent according to the Urbach rule. The relatively large Urbach-energy width and the high phonon-energy values lead to the conclusion that the absorption tail is the result of two effects: interaction of electrons/excitons with phonons as well as the static structural disorder which is associated with the existence of impurities and defects in the layered semiconductors.

## ACKNOWLEDGMENTS

The authors gratefully thank P. Schäfer for the EDX and electron microscope measurements and A. Wasnick for her assistance during the measurements. M. Moustafa wishes to express his appreciation to the Yousef Jameel Foundation for financial support.

<sup>1</sup>J. Yang, A. Banerjee, and S. Guha, *Appl. Phys. Lett.* **70**, 2975 (1997).

<sup>2</sup>X. Mathew, J. P. Enriquez, A. Romeo, and A. N. Tiwari, *Sol. Energy* **77**, 831 (2004).

<sup>3</sup>Z. Q. Li, Y. G. Xiao, and Z. M. Simon Li, *Phys. Status Solidi C*

**4**, 1637 (2007).

<sup>4</sup>S. J. Li, J. C. Bernede, J. Pouzet, and M. Jamali, *J. Phys.: Condens. Matter* **8**, 2291 (1996).

<sup>5</sup>D. N. Gujarathi, G. K. Solanki, M. P. Deshpande, and M. K. Agarwal, *Sol. Energy Mater. Sol. Cells* **90**, 2630 (2006).

- <sup>6</sup>H. Tributsch, *Appl. Phys. (Berlin)* **23**, 61 (1980).
- <sup>7</sup>H. Isomaki, J. von Boehm, and P. Krusiust, *J. Phys. C* **12**, 3239 (1979).
- <sup>8</sup>D. L. Greenaway and R. Nitsche, *J. Phys. Chem. Solids* **26**, 1445 (1965).
- <sup>9</sup>P. A. Lee, G. Said, R. Davis, and T. H. Lim, *J. Phys. Chem. Solids* **30**, 2719 (1969).
- <sup>10</sup>J. A. Wilson and A. D. Yoffe, *Adv. Phys.* **18**, 193 (1969).
- <sup>11</sup>R. Manzke and M. Skibowski, *Photoelectron Spectra of Layered Compounds*, Landolt-Börnstein, New Series, Group III, Vol. 23B, Pt. 84 (Springer-Verlag, Berlin, 1994).
- <sup>12</sup>R. H. Friend and A. D. Yoffe, *Adv. Phys.* **36**, 1 (1987).
- <sup>13</sup>A. H. Reshak and S. Auluck, *Physica B* **353**, 230 (2004).
- <sup>14</sup>R. B. Murray, R. A. Bromleyp, and A. D. Yoffe, *J. Phys. C* **5**, 3038 (1972).
- <sup>15</sup>D. W. Bullett, *J. Phys. C* **11**, 4501 (1978).
- <sup>16</sup>J. von Boehm and H. M. Isomaki, *J. Phys. C* **15**, L733 (1982).
- <sup>17</sup>H. P. Rimmington and A. A. Balchin, *J. Cryst. Growth* **21**, 171 (1974).
- <sup>18</sup>J. I. Pankove, *Optical Processes in Semiconductors* (Dover, New York, 1971).
- <sup>19</sup>C. Gaiser, T. Zandt, A. Krapf, R. Serverin, C. Janowitz, and R. Manzke, *Phys. Rev. B* **69**, 075205 (2004).
- <sup>20</sup>D. L. Greenway and G. Harbek, *J. Phys. Chem. Solids* **26**, 1585 (1965).
- <sup>21</sup>S. G. Patel, S. K. Arora, and M. K. Agarwal, *Bull. Mater. Sci.* **21**, 297 (1998).
- <sup>22</sup>F. Urbach, *Phys. Rev.* **92**, 1324 (1953).
- <sup>23</sup>H. Sumi and Y. Toyozawa, *J. Phys. Soc. Jpn.* **31**, 342 (1971).
- <sup>24</sup>B. Abay, H. S. Güder, H. Efeoglu, and Y. K. Yoğurtçu, *J. App. Phys.* **84**, 3872 (1998).
- <sup>25</sup>G. D. Cody, T. Tiedje, B. Abeles, B. Brooks, and Y. Goldstein, *Phys. Rev. Lett.* **47**, 1480 (1981).
- <sup>26</sup>C. H. Ho, Y. S. Huang, K. K. Tiong, and P. C. Liao, *Phys. Rev. B* **58**, 16130 (1998).
- <sup>27</sup>B. Abay, H. S. Güder, H. Efeoglu, and Y. K. Yoğurtçu, *J. Phys. Chem. Solids* **62**, 747 (2001).
- <sup>28</sup>Z. Yang, K. P. Homewood, M. S. Finney, M. A. Harry, and K. J. Resson, *J. Appl. Phys.* **78**, 1958 (1995).
- <sup>29</sup>S. Y. Hu, Y. C. Lee, J. L. Shen, K. W. Chen, K. K. Tiong, and Y. S. Huang, *Solid State Commun.* **139**, 176 (2006).